The effect of nearby bubbles on array gain

R. Lee Culver[a] and J. Daniel Park
Applied Research Laboratory, The Pennsylvania State University, State College, Pennsylvania, 16801

Timothy G. Leighton and David G. H. Coles
Institute of Sound and Vibration Research, University of Southampton, Highfield S017 1BJ, United Kingdom

(Received 8 April 2011; revised 11 October 2011; accepted 11 October 2011)

The coherent processing of signals from multiple hydrophones in an array offers improvements in angular resolution and signal-to-noise ratio. When the array is steered in a particular direction, the signals arriving from that direction are added in phase, and any signals arriving from other directions are not. Array gain (AG) is a measure of how much the signal arriving from the steering direction is amplified relative to signals arriving from all other directions. The subject of this paper is the manner in which the AG of an acoustic array operating in water that contains air bubbles is affected by scattering from nearby bubbles. The effects of bubbles on acoustic attenuation and dispersion are considered separately from their effects on AG. Acoustic measurements made in bubbly water using the AB Wood tank at the Institute of Sound and Vibration Research, University of Southampton, in June 2008 show that as bubble density increases, relative phase shifts in individual hydrophone signals increase and signal correlation among the hydrophones is reduced. A theory and numerical simulation linking bubble density at the hydrophone to the AG is in good agreement with the measurements up to the point where multiple scattering becomes important.
 [DOI: 10.1121/1.3658473]

PACS number(s): 43.60.Fg, 43.30.Re, 43.60.Cg [EJS] Pages: 3812–3826

I. INTRODUCTION

It is well known that gas bubbles in water scatter and attenuate sound and can greatly affect acoustic propagation (e.g., Refs. 1 and 2). The magnitude of these effects depends on the relationship between the acoustic wavelength and the size of the bubbles, as well as the density of the bubbles. In addition, when hydrophones are used in the vicinity of air bubbles, scattering by nearby bubbles can alter the phase and amplitude of the received signals. In this way, bubble scattering can reduce signal correlation between hydrophones and thus reduce beamformer and array gain, and that is the subject of this paper.

The analysis presented here depends upon the following assumptions. First, because the hydrophone spacing is much smaller than the dimensions of the bubble cloud, we assume that the bulk effects of the bubble cloud to attenuate signals and modify sound speed are applied equally to all hydrophones. This means that bubble cloud-induced signal attenuation and dispersion will not affect array gain as long as the attenuation is not so great as to reduce signal power at the array output to less than about 10 dB above the noise power. Second, we assume that bubble-induced changes in hydrophone sensitivity affect all of the hydrophones equally. The analysis here is applied to signal and noise power after transduction and thus will not be affected by sensitivity changes that have occurred equally to all transducers. If either of these assumptions are not valid, then the effects of dispersion, attenuation, and sensitivity changes could further degrade beamformer and array gain in a manner that we have not considered in this paper.

Array signal processing (or beamforming) exploits the spatial coherence (or compactness) of the signal and the spatial incoherence (or spread) of the noise. Beamforming provides an increase in the signal to noise ratio when the signal arrives from one direction only (i.e., is spatially compact or coherent), while the noise or interference arrives from many directions (i.e., is spatially incoherent or at least less coherent). If necessary, the main beam of the array can be steered toward the direction of the acoustic signal arrival either by physically changing the orientation of the array or by adjusting (delaying or advancing) each of the outputs from the individual elements in the receive array so as to align their phases. The array gain (AG) is a measure of how much beamforming improves the ratio of signal power to noise power relative to that at the output of a single hydrophone. Expressed in dB, AG is $10\log_{10}$ of the linearly-expressed signal-to-noise power ratio (SNR) at the array output divided by that at the array input:[3,4]

$$AG = 10\log_{10}\left\{\frac{SNR_{\text{array output}}}{SNR_{\text{array input}}}\right\} \tag{1}$$

where

$$SNR = \frac{\text{signal power}}{\text{noise power}}. \tag{2}$$

In general, power is the squared magnitude of the appropriate bin of the discrete Fourier transform (DFT) of the output of a hydrophone or the beamformer (a digitized voltage). Signal power is obtained when signal is present at the

[a]Author to whom correspondence should be addressed. Electronic mail: rlc5@psu.edu

hydrophones; noise power otherwise. Although AG is the appropriate measure for quantifying array performance, it depends upon the directional characteristics of the noise field. Accordingly, we investigate the effects of bubbles on beamformer gain (BG), which is the gain in signal or noise power provided by beamforming, and then predict AG when the noise is uncorrelated across the array. Equations (1) and (2) can be combined to relate AG to BG:

$$AG = 10\log_{10}\left\{\frac{\text{signal power @ array output}/\text{noise power @ array output}}{\text{signal power @ single hydrophone}/\text{noise power @ single hydrophone}}\right\}$$
$$= 10\log_{10}\left\{\frac{\text{signal power @ array output}}{\text{signal power @ single hydrophone}}\right\} - 10\log_{10}\left\{\frac{\text{noise power @ array output}}{\text{noise power @ single hydrophone}}\right\} = BG_{\text{signal}} - BG_{\text{noise}}, \quad (3)$$

where BG_{signal} and BG_{noise} refer to gains against signal and noise, respectively. In this paper the beamformer simply sums the hydrophone outputs. Therefore, if the signal is perfectly coherent across all hydrohones, the signal power at beamformer output will be N^2 times the signal power at the output of a single hydrophone so that $BG_{\text{signal}} = 10\log_{10} N^2$ (N is the number of hydrophones). If the noise is completely uncorrelated (i.e., the phase is random) across all of the hydrophones, then the expected value of the noise power at the beamformer output will be N times the noise power at a single hydrophone output, so that in the mean, $BG_{\text{noise}} = 10\log_{10} N$. As an example, for a three element array, perfectly correlated signal and completely uncorrelated noise, $BG_{\text{signal}} = 10\log_{10}(9) = 9.5$ dB, $BG_{\text{noise}} = 10\log_{10}(3) = 4.75$ dB, and $AG = 9.5 - 4.75 = 4.75$ dB, which is equal to $10\log_{10} N$. When the signal is not perfectly correlated across the array, BG_{signal} will be less than $10\log_{10} N^2$. When the noise is not completely uncorrelated across the array, BG_{noise} will be greater than $10\log_{10} N$. In either event, AG will be less than $10\log_{10} N$.

The objective of this research was to understand and quantify whether the effect of the bubbly wake on the AG provided by a line array of hydrophones towed at shallow depth behind a surface ship would simply attenuate sound and thus reduce SNR at all elements, or would there be, in addition, some adverse effect on the AG? For example, would scattering by the bubbles add correlated interference to the array elements, or would it reduce signal correlation across the array?

The first step toward answering these questions was to find an applicable theory. In a sufficiently diffuse distribution of bubbles, acoustic propagation can be described using the "first-order multiple scattering" model presented in Chapters 4 and 6 of Ishimaru.[5] Single scattering is similar to the Born approximation, in which the field incident on a bubble is approximated by the attenuated incident field. The approximation is valid if at least one of the following conditions is satisfied. First, the albedo (ratio of the scattered power to the total incident power) must be much smaller than one. Second, the optical distance (the integral of bubble density times the extinction cross section) must be much smaller than one. Third, the receiver must have a narrow angle. The measurements reported in this paper satisfy all but the third criterion. The received field is composed of the coherent sum of an attenuated direct path arrival and attenuated signals scattered by each of the bubbles. Ishimaru postulates that the field scattered by different bubbles is, on average, uncorrelated and derives Eq. (6-11) for $B(r_1, r_2)$ the spatial correlation of the scattered contribution to the field at points r_1 and r_2. With the further assumption that no bubbles are close to the receiver, Ishimaru derives Eq. (6-17) (repeated below):

$$B(d) = \frac{\sigma_s}{2\sigma_t}\int_0^{\pi/2} g(\gamma,\theta) J_0(kd\sin\theta)\,\sin\theta\,\mathrm{d}\theta. \quad (4)$$

Here d is the distance between points r_1 and r_2, J_0 is the zero-order Bessel function of the first kind, θ is measured from the plane between points r_1 and r_2, σ_s and σ_t are the scattering and total cross-sections of a single bubble, respectively, and γ is the attenuation coefficient along the path to the bubble (discussed further below). The function $g(\gamma,\theta)$ is defined by

$$g(\gamma,\theta) = \frac{\exp(-\gamma) - \exp(\gamma/\cos\theta)}{1 - \mathrm{j}\cos\theta}. \quad (5)$$

Note that Ainslie and Leighton have provided corrected expressions for the damping constants which are required to calculate σ_s and σ_t.[6]

An initial effort was to numerically integrate Ishimaru's equation [Eq. (6-11)] using random distributions of bubbles in the volume separating the projector and hydrophone but with no bubbles close to the hydrophones. This result matched Eq. (4), thus validating that approximation.[7] However, when bubbles were placed closer to the hydrophone, the numerical result did not match Eq. (4). The spatial correlation of the scattered field remained high despite increasing hydrophone separation, which is inconsistent with the Bessel function in Eq. (4). This led to a hypothesis that bubbles near the hydrophones would add correlated interference and thus reduce the gain normally provided by beamforming.

By good fortune, the Office of Naval Research was willing to fund a direct measurement of bubble scattering effects on an array in order to test the hypothesis and numerical prediction. An opportunity to conduct the measurement was provided by the Institute of Sound and Vibration (ISVR), University of Southampton using the A B Wood acoustic tank, which has been fitted with a means of generating clouds of small bubbles.[8]

In June 2008, an acoustic source and a 3-element hydrophone array were used to measure the characteristics of acoustic propagation as bubble density at the array changed. Acoustic frequencies between 25 kHz and 35 kHz were employed. As shown in Sec. III, the phase and amplitude of the received signal with and without bubbles nearby indicates that increasing bubble density at the array reduces the correlation between signals received at the different hydrophones.

This result pointed to a mechanism that differed from that predicted by the earlier numerical results, so the first-order multiple scattering model was revisited. A numerical simulation was developed to calculate the received signals at the hydrophones by coherently summing the direct path and bubble scattered signals. Bubbles were positioned randomly around the hydrophones at distances reflective of the bubble density. Section VI presents distributions of the phases of the received signals calculated using the numerical simulation. The agreement between the measurements and the numerical results is discussed in Sec. VII.

Note that the AB Wood experiment included a separate measurement to estimate the density of the bubbles in the tank. Acoustic attenuation measured over several paths through the bubble cloud and used to estimate the bubble density integrated over those paths. A Gaussian spatial bubble distribution was fitted to the integrated bubble densities, and the bubble density at specific points within the cloud was obtained. These results are presented in Secs. IV and V.

II. BEAMFORMER GAIN MEASUREMENTS

A. Measurement setup

The AB Wood water tank measures 8 m × 8 m × 5 m (l·w·d). Figure 1 shows the measurement hardware, which was positioned approximately in the tank center, near the source of small bubbles located at the tank bottom. A means of generating small (10 μm – 400 μm) air bubbles such as those found in the ocean is an important capability of the AB Wood facility. For example, see Fig. 5 of Ref. 8. Air bubbles are generated using a venturi and then directed into a smaller tank approximately 1.2 m × 2 m × 1.2 m in size which allows the larger bubbles to rise to the surface. The water in the smaller tank turns a milky color due to the many small bubbles. Bubbly water containing only smaller bubbles is then pumped from the smaller tank into the AB Wood tank and discharged through a diffuser placed on the bottom near the center of the tank. The discharged bubbles form a roughly conical cloud as they rise slowly to the surface. Although the instantaneous distribution of the bubbles varies with time in a random fashion, the statistics of bubble density are assumed to be stationary in time.

The acoustic measurement reported here utilized a locally manufactured directional acoustic projector pointed horizontally and placed approximately 3 m from the center of the bubble cloud and 1.9 m below the water surface. The projector provides relatively flat source level over a large frequency band, varying by less than 15 dB from 25 kHz to 120 kHz. The projector position was fixed, and the main beam was directed toward the center of the bubble cloud. At 30 kHz, the projector has a 3 dB beamwidth of 27.7°, and a sidelobe at 50° which is 24 dB down. In addition to the direct path through the main lobe, the measurement geometry results in a surface bounce path that leaves the transducer at 52° angle and arrives about 1.2 ms after the direct path. This angle is within the projector sidelobe, but the transmit level is 24 dB lower than the main beam level. Thus the surface bounce path is not expected to interfere with the direct path signal, and the results shown below seem to bear this out.

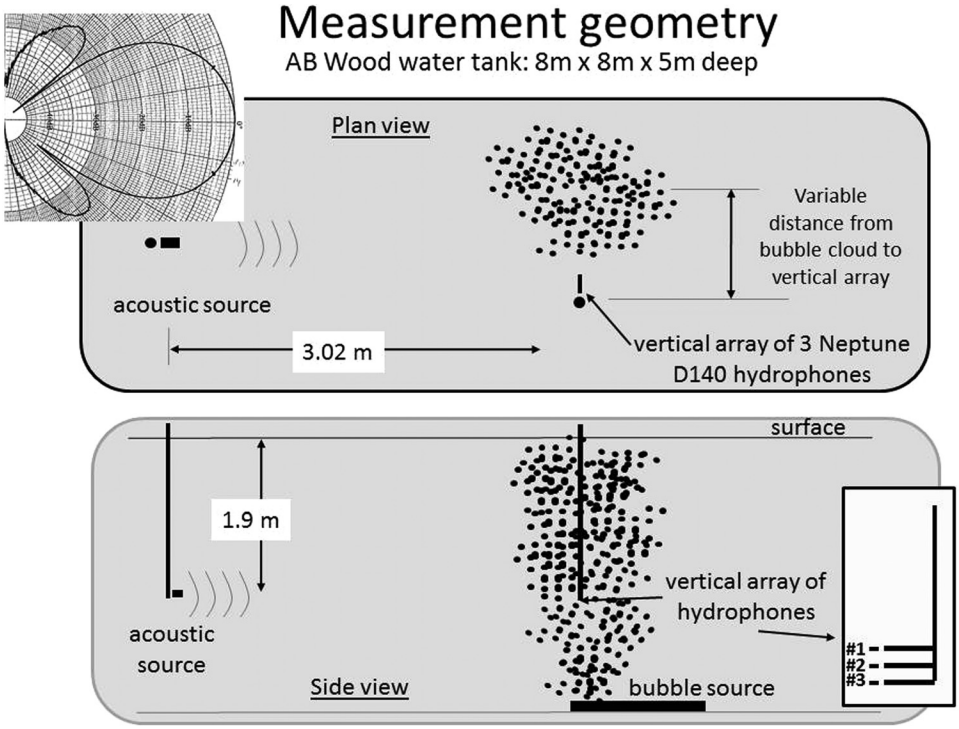

FIG. 1. Geometry for beamformer gain measurements. The upper panel shows a view looking down on the tank and the vertical hydrophone array. Moving the hydrophone array closer to the bubble cloud center results in increased bubble density at the array. The projector beam pattern @ 30 kHz is shown in the inset. The 3 dB beamwidth is 27.7° and there is a −24 dB sidelobe at 50°. The bottom panel shows a side view of the geometry. Details of the hydrophone array are shown in the inset in the bottom panel.

A 3-element vertical line array of Neptune D140 hydrophones was located at the same depth as the projector and at a variable distance from to the bubble cloud center. The hydrophones are omnidirectional up to 160 kHz. To form the array, they were spaced 0.025 m vertically, with the middle hydrophone placed at 1.94 m depth. The array element spacing is approximate (acoustic wavelength)/2 at 30 kHz, however the noise field was found to be correlated between the elements at all frequencies used in the acoustic measurement. Bubble density at the three element array was increased (or decreased) by moving the array closer to (or farther from) the bubble cloud.

The acoustic frequencies used in the array gain measurement were 25 kHz, 30 kHz, and 35 kHz. About 120 transmissions were made at each position of the array and at each frequency. The transmit signal was a 3 ms pulse composed of a 1 ms ramp-up, a 1 ms constant amplitude portion, and a 1 ms ramp down. Received signals were sampled at 250 kHz. A measurement made with the bubble generator off showed little variability and thus utilized 24 transmissions at 30 kHz only.

Signals were transmitted with the vertical array positioned at four different distances from what was estimated by eye to be the bubble cloud center: (1) 0 cm, (2) 30 cm, (3) 60 cm, and (4) 90 cm. Subsequent to the AG measurements and as discussed in the next section, acoustic attenuation was measured in the plane of the acoustic source and hydrophone array in order to estimate bubble density, and the center of the bubble cloud was found to be displaced about 30 cm from the assumed location. This result has been accounted for in the results reported here.

B. Measurement results

Figure 2 shows received signals at two distances the bubble cloud (and thus, two different bubble densities). With the array 60 cm from the center of the bubble cloud (left panel), the amplitude and phase of the signals are very similar for all three hydrophones. However, when the array is moved 30 cm closer to the bubble cloud center (right panel), differences in amplitude and phase at the hydrophones are evident. Note too that there is no indication of interference by a surface bounce arrival.

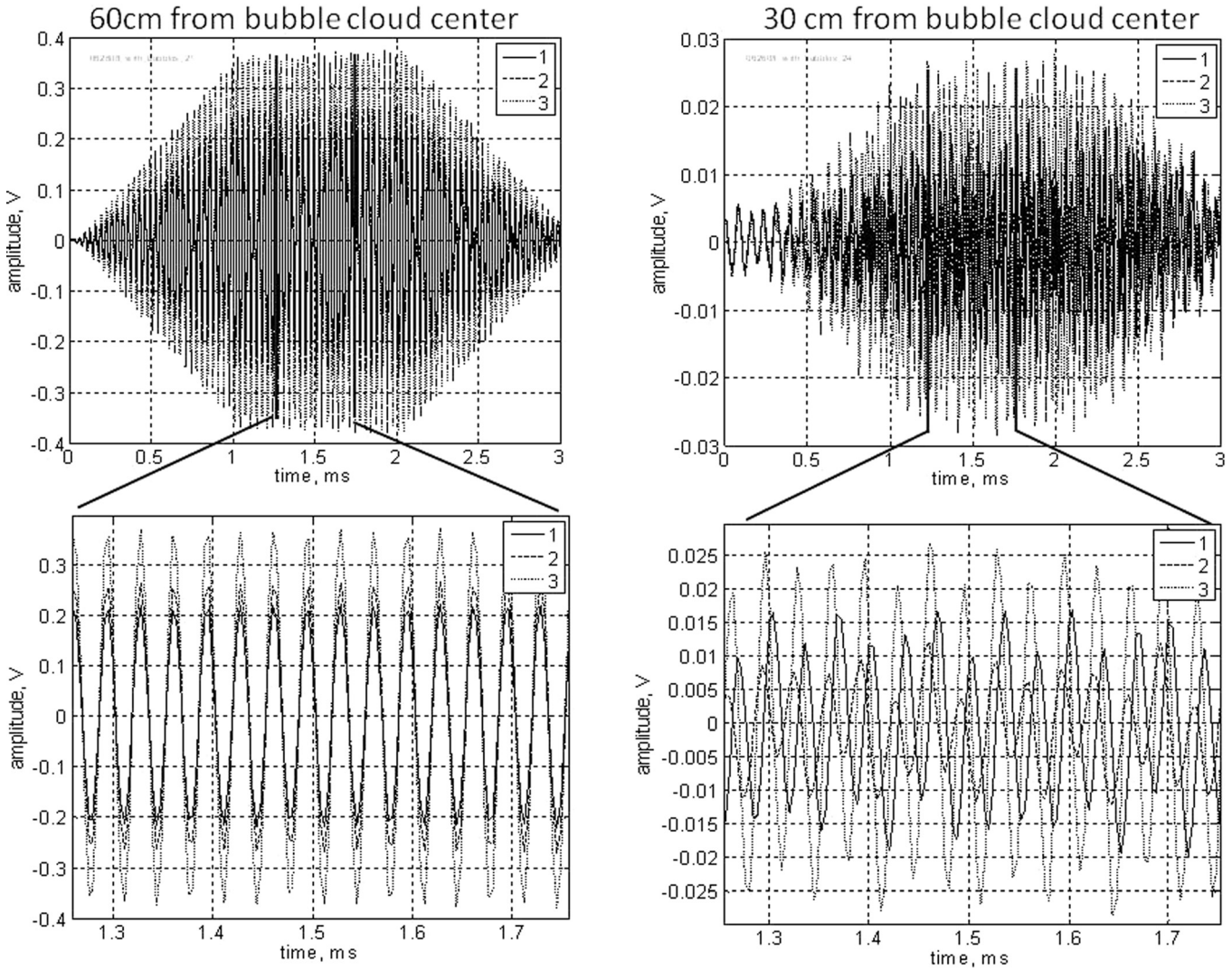

FIG. 2. Signals received at hydrophones 1, 2 and 3 with the array at two different distances from the bubble cloud center. The right panel corresponds to a higher bubble density at the receive array and displays larger phase differences between the signals.

One set of acoustic measurements were made before introducing bubbles into the tank and with the hydrophone array positioned 60 cm from the assumed center of the bubble cloud (had it been present). This result is referred to as the "no-bubble" case. When no bubbles are present, assuming all hydrophones have the same phase response, any difference in signal phase among the hydrophones is solely due to array tilt. In the presence of bubbles, however, phase differences could also be caused by superposition of bubble-scattered signals at the hydrophone, or possibly by differences in sound speed along the two paths. However, because the hydrophones are so close together (2.5 cm separation) relative to the path length (2 m) and bubble cloud size (1 m), we assume that sound propagating from the projector to the two hydrophones passes through virtually the same medium and experiences the same propagation speed and attenuation. Bubble scattering is left as the primary cause of phase differences. Also, we hypothesize that since the bubbles are randomly distributed in space, phase differences induced by bubble scattering should average to zero. Thus, the mean of measured phase differences, if non-zero, indicates that the array is tilted. This is consistent with the observation that the mean phase difference is seen to increase linearly across the array (this result is not shown in the paper).

A measurement of maximum beamformer gain requires that the array be steered in the direction of the arriving signal. As shown in Fig. 1, the hydrophone array was attached to a long rod suspended from rails laid across the tank opening. This arrangement resulted in the hydrophone array sometimes being tilted a few degrees from the vertical. The phones were moved a number of times for different measurements and the array may or may not have been tilted slightly for a particular measurement. Therefore, when necessary, the mean phase difference was set to zero to correct for array tilt.

The discrete Fourier transform (DFT) method was used to estimate signal phase using the 1-ms (250 point) constant amplitude portion of each received signal.[9] The complex DFT coefficient $X(m)$ taken from the proper frequency bin contains the signal amplitude and phase. The power at a single hydrophone is the squared magnitude $|X(m)|^2$. The power at the beamformer output is $|X_1(m)+X_2(m)+X_3(m)|^2$, where the subscript indicates hydrophone number and signal phase alignment to account for array tilt is assumed.

The upper four panels of Fig. 3 show individual hydrophone and beamformer output power measured at 30 kHz for the no-bubble case. Panel (a) compares the power in the received signal for the three hydrophones with the beamformer output. There is no ping-to-ping variation due to high SNR and no interference from bubble scattering. Panel (b) shows the gain provided by beamforming when no bubbles are present, which is the difference between the two lines in panel (a). The measured value matches the theoretical prediction of $10 * \log_{10}(3^2) = 9.5$ dB. Panel (c) shows the hydrophone and beamformer output power measured 10 ms prior to the signal arriving. These levels represent the background noise present in the AB Wood tank. From panel (a) the single hydrophone signal power is about 40 dB, while (from panel (b)) the single hydrophone noise power is about −40 dB, so that the SNR for a single hydrophone is about 80 dB for this no-bubble case. In panel (d) the solid line shows the beamformer gain against noise, which is the difference between the beamformer output and the (linearly) averaged hydrophone power in panel (c). The beamformer gain against noise is quite variable; the (linearly) averaged gain (dashed line) is about 7.8 dB.

That $BG_{\text{noise}} \approx 7.8$ dB in panel (d) of Fig. 3 indicates that the noise is not completely uncorrelated across the array. The theoretical prediction for uncorrelated noise is $10 * \log_{10}(3) = 4.75$ dB. Using Eq. (3), the mean AG calculated for the no-bubble case is $(9.5 - 7.8) = 1.7$ dB. The AG in uncorrelated noise would be $(9.5 - 4.75) = 4.75$ dB.

Note, that the mean measured AG is less than 4.7 dB not because the signal is less than perfectly coherent across the array, but because the noise is not completely incoherent across the array. The source of correlated noise at 30 kHz in the AB Wood tank is unknown, but it is virtually unchanged for all of the measurements, with and without bubbles present and regardless of the array proximity to the bubble cloud.

The lower four panels of Fig. 3 show the signal and noise power and beamformer gains for 30 kHz with bubbles present and the array 30 cm from the bubble cloud center. The signal levels at a single hydrophone and at the beamformer output are significantly lower and more variable than for the no-bubble case [panel (e)], but the noise levels (single hydrophone and beamformer output) are not that different [panel (g)]. The BG_{noise} is still about 6.9 dB [panel (h)], however the BG_{signal} has dropped to about 6.5 dB [panel (f)]. While the presence of bubbles close to the array has not had much effect on the correlation of the noise, it has caused a significant drop in signal correlation across the array. The mean AG calculated for this case is −0.4 dB, which means that the beamformer is actually reducing mean SNR.

Histograms of BG_{signal} for three measurement frequencies and different bubble densities are shown in Fig. 4. The columns correspond to measurements made at (left to right) 25 kHz, 30 kHz, and 35 kHz. The upper three rows correspond to measurements made with the array at (top to bottom) 30 cm, 60 cm and 90 cm from the center of the bubble cloud. The bottom panel is the no-bubble case.

Figure 4 shows that as the array is moved closer to the center of the bubble cloud and thus, the bubble density at the array increases, the distribution of BG_{signal} becomes more and more spread out. Also, the mean BG_{signal} drops from 9.5 dB, the maximum value for perfectly correlated signals, to approximately 6.5 dB as the array moves closer to the bubble cloud center.

The reduction in BG_{signal} is due to differences in signal phase among the hydrophones, histograms of which are shown in Fig. 5. The arrangement of the columns and rows are the same as in Fig. 4. The mean phase difference is zero because the array is steered toward the projector.

The distribution of the phase difference is very narrow for the no-bubble case (bottom panel); it is essentially a delta function. As the array is moved closer to the bubble cloud center and the bubble density increases (moving up in the figure), the variance of the phase difference increases and the histograms flatten out. The phase difference approaches

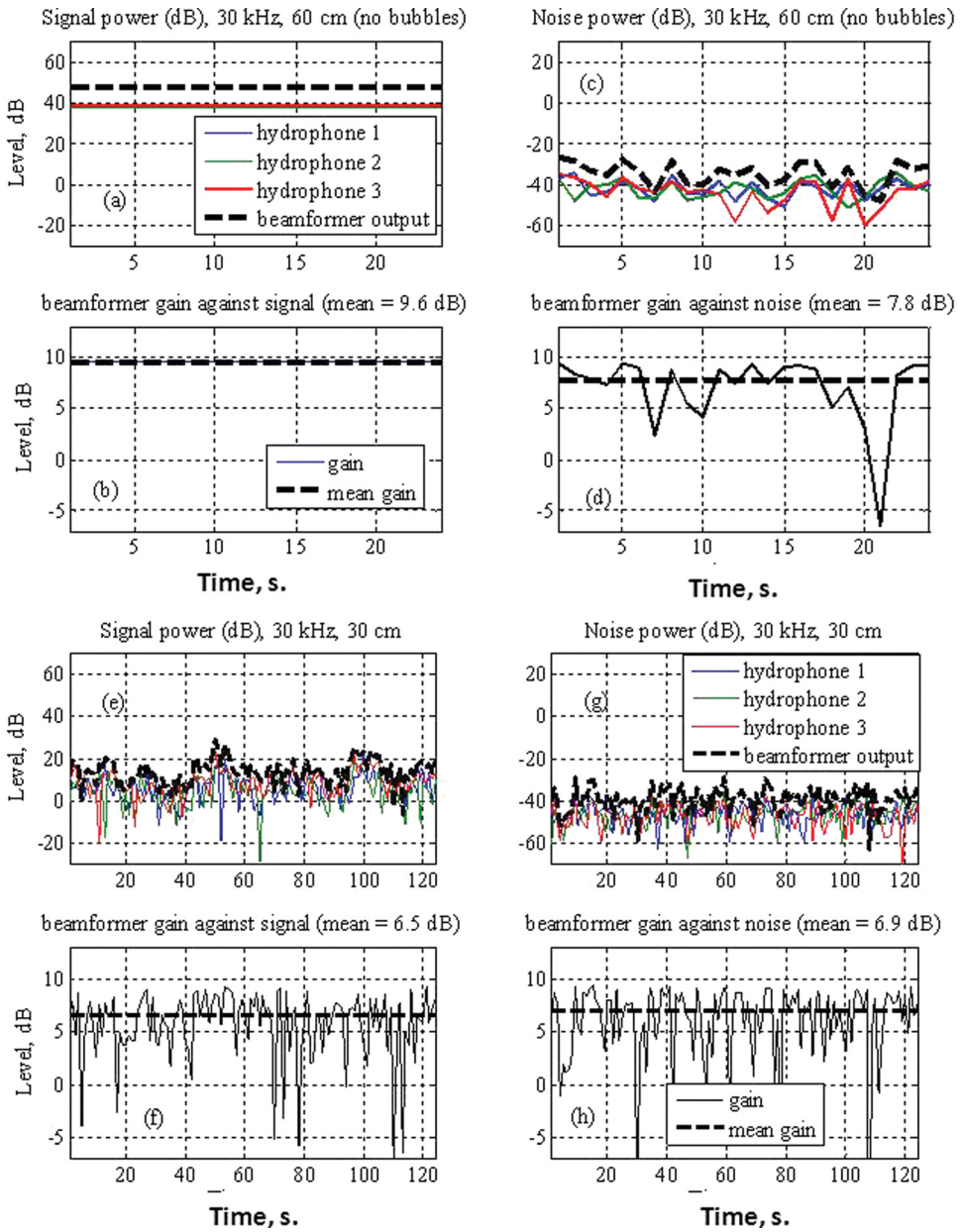

FIG. 3. (Color online) Signal and noise power at the individual hydrophones and at the beamformer output for the no bubble case [panels (a) – (d)] and for the array 30 cm from the bubble cloud center [panels (e) – (h)]. Panels (a), (c), (e), and (g) show signal and noise power at the hydrophones and beamformer output. Panels (b), (d), (f), and (h) show beamformer gain against signal and noise.

a uniform distribution in the top row, which corresponds to when the array was closest to the bubble cloud center.

The von Mises distribution has been used to describe the phase distribution of the superposition of sinusoidal signals affected by weak scatterering.[10] Also, the probability density function of the total phase of a random sinusoid in the weak-scatterer case has been derived.[11] In Ref. 11, the phases of the individual sinusoids are assumed to possess a von Mises probability density function as well. The closed form expression for the von Mises distribution of phase angles x is given by

$$f(x|\mu,\kappa) = \frac{e^{\kappa\cos(x-\mu)}}{2\pi I_0(\kappa)} \tag{6}$$

where the parameters μ and κ are analogous to the mean and inverse variance of the distribution. The phase distributions shown in Fig. 5 all can be fitted by the von Mises function.

III. BUBBLE DENSITY MEASUREMENTS

This section describes measurements that were made to estimate bubble density at the locations of AG measurements. Bubble density measurements were made in the same environment (physically) as the AG measurements, i.e., the same bubble generation and injection procedures were followed, so that the bubble clouds would be statistically identical. The same projector and hydrophones were used for both measurements. The projector and hydrophones were placed at the same depth as for the AG measurements. However, the hydrophones were removed from the array fixture used in the AG measurements and placed at separate locations at the same depth as the projector. The distances between the projector and hydrophones varied from 2.0 to 3.0 meters. Tone bursts 3 ms long (unshaded) at 2 kHz steps from 25 kHz to 99 kHz were transmitted in order to estimate bubble density over a range of radii. Approximately ten pings were transmitted at each frequency. Only the 30 kHz measurements were used to

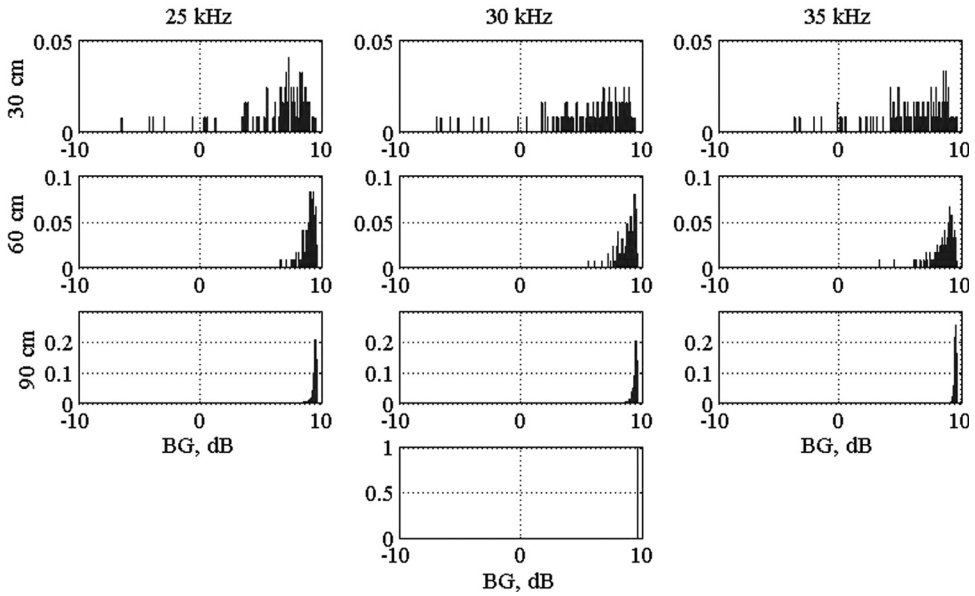

FIG. 4. Histograms of BG_{signal}, the beamformer gain against signal. The columns correspond to frequencies of (left to right) 25 kHz, 30 kHz, and 35 kHz. The upper three rows correspond to measurements made with the array at (top to bottom) 30 cm, 60 cm, and 90 cm from the center of the bubble cloud. The bottom panel is the no-bubble case. Note that the vertical scales are different among the panels.

estimate the spatial extent of the bubble cloud. The sample rate for the bubble density measurement was 2 MHz.

The measurement geometry is shown in Fig. 6. Bubble density measurements were made with hydrophones at the locations marked 1A, 2A, 3A, …, 3D. Locations 2B, 2C, and 2D (marked with squares) are 30, 60, and 90 cm from the (initially assumed) bubble cloud center and are the positions of the AG measurements discussed in the previous section. The filled circles and squares indicate the density measurement that were used to find the best fit bubble cloud as described below. Open circles and squares indicate positions that were not used to estimate bubble density because they were outside the main lobe of the projector beam pattern at 30 kHz. Position 2A was initially thought to be on the vertical axis of the bubble cloud. However, based upon the density measurements, the bubble cloud center was eventually estimated to be at the location indicated by the star. The bubble cloud appears to be wider in the direction of the bubble diffuser axis. Dashed lines are the estimated axes of the bubble cloud.

The number of bubbles along the propagation path that are resonant at a particular frequency can be deduced from the acoustic attenuation, which is estimated by subtracting the received signal level when the bubble cloud is present from the received level without the bubble cloud present. Received levels were estimated using 20 $\log_{10}$ of the magnitude of the appropriate DFT bin. The only locations at which the received levels were measured with no bubbles present

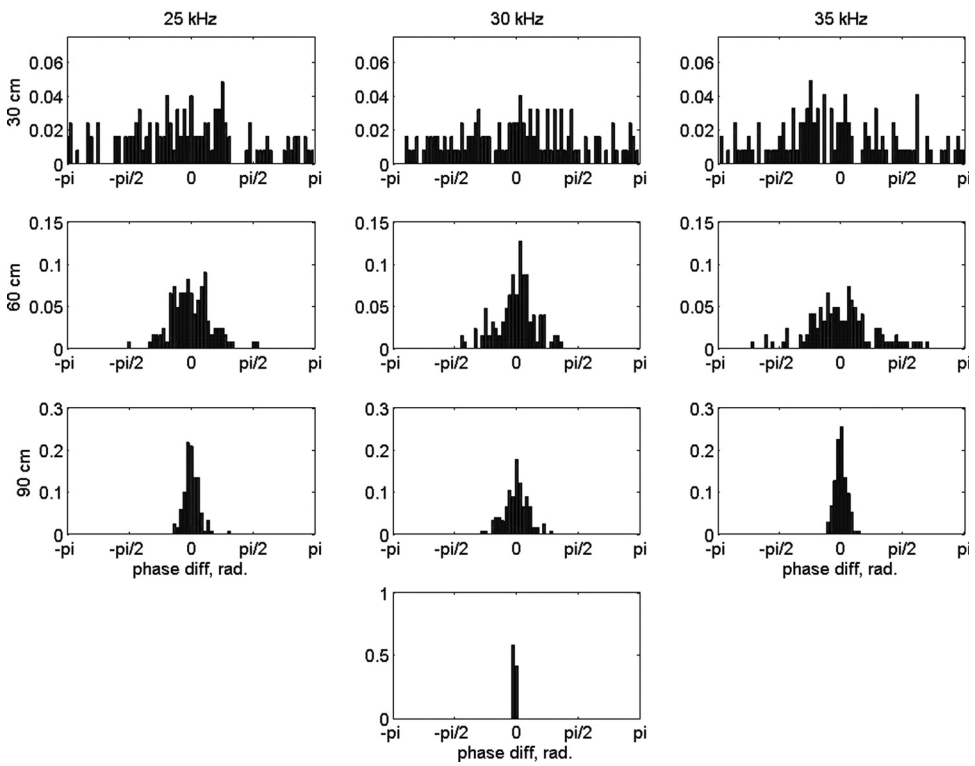

FIG. 5. Histograms of the phase difference between signals received at hydrophones 1 and 2. The columns correspond to frequencies of (left to right) 25 kHz, 30 kHz, and 35 kHz. The upper three rows correspond to measurements made with the array at (top to bottom) 30 cm, 60 cm, and 90 cm from the center of the bubble cloud. The bottom panel is the no-bubble case. Note that the vertical scales are different among the panels.

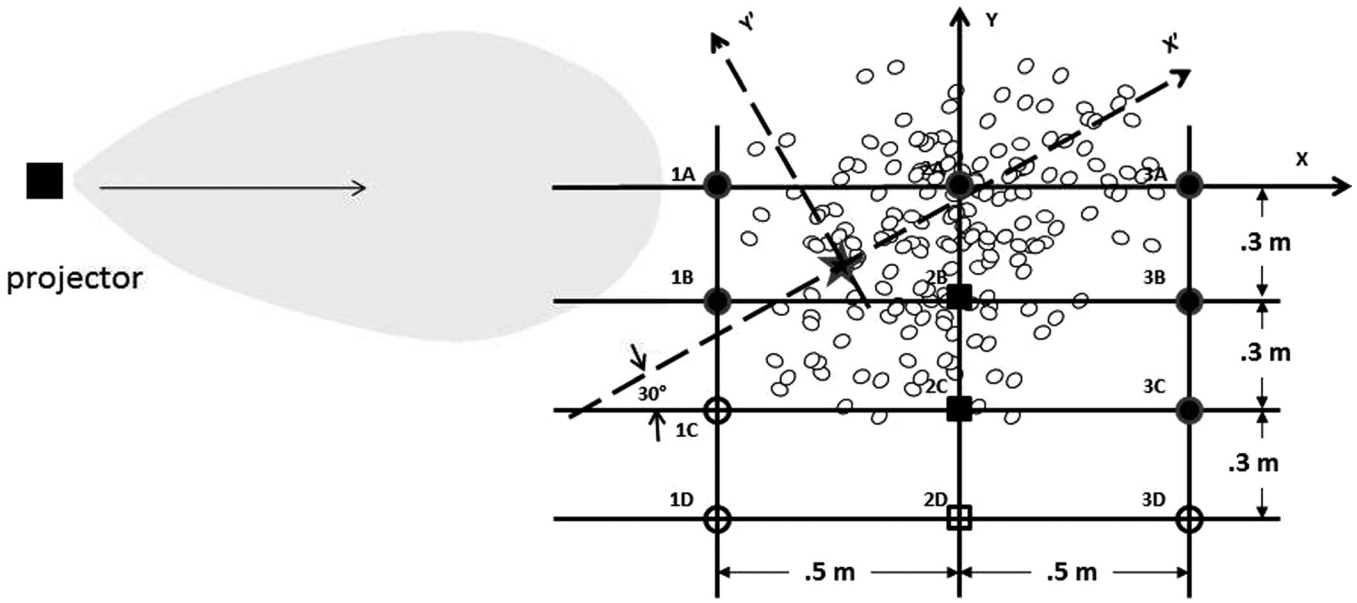

FIG. 6. Geometry used to measure bubble density. Points 1A, 2A and 3A, …, 3D indicate the positions of single hydrophone attenuation measurements. Filled circles and squares indicate the positions of density measurements that were used to find the best fit bubble cloud. The star marks the estimated location of the vertical axis of the bubble cloud. The dashed lines are the axes of the bubble cloud, which are assumed to be oriented by the bubble diffuser.

were 1A, 2A, and 3A. No-bubble received levels for the other locations were estimated using these measurements and correcting for the projector beam pattern and the distance from the projector to the location. Bubble densities were estimated from the attenuation measurements using the method presented by Ref. 12.

The radius of the bubble (in meters) that is resonant at frequency f_R (in Hz) can be calculated using Eq. 6.3.11 from Ref. 1,

$$a = \frac{1}{2\pi f_R}\left(\frac{3\gamma P_A b\beta}{\rho_A}\right)^{1/2} \tag{7}$$

where γ is the dimensionless ratio of specific heats for the gas [not the same as the γ appearing in Eq. (4)], P_A is the ambient pressure ($\mathrm{N/m^2}$), ρ_A is the ambient density of water ($\mathrm{kg/m^3}$), and b and β are functions that correct for the adiabatic assumption and surface tension. For the frequencies of primary interest to the present work, $f_R = 25$, 30, and 35 kHz, the corresponding bubble radii a at 2 m depth are 142, 118 and 102 μm, respectively.

Each attenuation measurement corresponds to the total path from the projector to the hydrophone. Therefore, the bubble density estimated from each attenuation measurement corresponds to the density integrated over the projector-to-hydrophone path. Bubble density is usually expressed in units of $\mathrm{m^{-3}}$ in a 1 μm bin, which means that bubble density integrated along a path would have units of $\mathrm{m^{-2}}$ in a 1 μm bin. As an example, Fig. 7 shows bubble densities estimated for propagation paths between the projector and

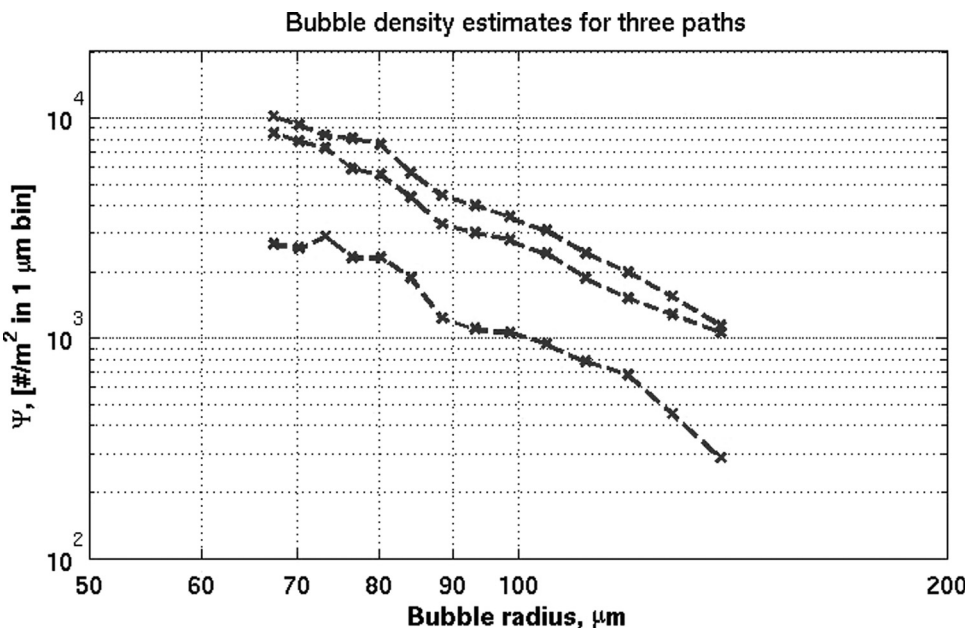

FIG. 7. Bubble size distributions estimated for hydrophone locations (top to bottom curve) 3A, 2A, and 1A. The corresponding projector-to-receiver path length are 3.5 m, 3 m, and 2.5 m, respectively.

hydrophones at locations 3A, 2A, and 1A, respectively (top to bottom). The corresponding path lengths are 3.5 m, 3.0 m, and 2.5 m, respectively. The upper curve is associated with the longest path, while the middle and lower curves indicate fewer bubbles and are associated with shorter path lengths. All bubble density estimates appear to display a power law dependence on radius with an exponent of approximately −3.3. For comparison, the oceanic bubble size distributions summarized by Leighton *et al*. (Fig. 5 of Ref. 8) display an approximate power law dependence with a coefficient of approximately −3.0 to −3.3.

Using the integrated bubble densities along the projector-to-hydrophone paths, the next step is to calculate the spatial distribution of the bubble density in the plane of the projector and hydrophones. This is accomplished by assuming that the mean bubble density obeys a two-dimensional Gaussian spatial distribution in the horizontal plane. Bubbles of all radii are assumed to have the same spatial distribution, but only bubble density derived from the 30 kHz measurements were used to estimate the spatial distribution. There are five parameters associated with the Gaussian spatial distribution: the coordinates of the bubble cloud center, the standard deviations of the bubble density in each direction, and the orientation of the distribution axes (a single angle). The bubble cloud center and density standard deviations were estimated from the bubble density measurements. The angle of the distribution axes was taken to be 30° because that is the orientation of the bubble diffuser.

The search for the unknown parameters was accomplished as follows. Two-dimensional Gaussian distributions were calculated for each set of possible parameter values. The modeled Gaussian distributions were then summed along the direction parallel to the line 1A – 3A to obtain two-dimensional surfaces that are proportional to the cumulative sum of the bubbles between the projector and a point along the projector-hydrophone path. The cumulative distributions were then normalized to have a maximum value of one. For the measurement results, the integrated bubble densities corresponding to the locations marked by filled circles and squares in Fig. 6 were normalized by the maximum value. The mean difference between the measured and modeled cumulative bubble sums was calculated by subtraction, and the mean squared difference calculated. The parameter set corresponding to the smallest mean squared difference was selected as the best fit.

The location of the center of the best fit bubble cloud center was found to be ($x = -0.2875$ m, $y = -0.2375$ m), which is marked by a star in Fig. 6. The standard deviations of bubble density were estimated to be $\sigma_{x'} = 0.3766$ m, $\sigma_{y'} = 0.3688$ m in the directions of the dashed lines shown in Fig. 6. The mean square difference between the best fit and the measured bubble density based upon the 30 kHz attenuation measurements was 0.0132.

The bubble densities at the locations identified in Fig. 6 as 2B, 2C, and 2D (corresponding to 30 cm, 60 cm, and 90 cm from the center of the bubble cloud in the AG measurements) for the three bubble sizes of interest are given in Table I. The units of bubble density in Table I are m^{-3} in a 1 μm bin. These are the bubble densities against which the AG measurements are plotted in the next section. Note that strictly speaking, the number of bubbles at a single radius is zero. The densities reported in Table I could be interpreted as the number of bubbles with radius 142, 118 and 102 μm ± 5 μm, where the range of radii is estimated from the 3 dB width of the resonant peak calculated assuming a bubble quality factor Q of ten.

TABLE I. Estimated bubble density (units: m^{-3} in a 1 μm bin) at the middle hydrophone of the array at specified distances from what was originally thought to be the center of the bubble cloud.

	35 kHz (102 ± 5 μm)	30 kHz (118 ± 5 μm)	25 kHz (142 ± 5 μm)
30 cm	4100	2300	1000
60 cm	2700	1300	400
90 cm	1000	400	50

IV. BEAMFORMER GAIN VS BUBBLE DENSITY

Figure 8 shows the mean beamformer gain for the signal, BG_{signal}, at 30 kHz (i.e., the mean of the center column of Fig. 4) plotted against the bubble densities given in Table I for 30 kHz (118 μm bubbles). The mean BG_{noise} at 30 kHz is also shown. The measured beamformer gains for the no-bubble case are plotted versus the calculated bubble density at 150 cm from the bubble cloud center, which was about 8 $(\Psi(a)\Delta a)^{1/3}$, where Δa is the bubble resonance width. The gain against the signal decreases relatively slowly over about a 500-fold increase in bubble density, but drops quickly when the density increases by about another factor of six (from about 400 to about 2300). The critical density above which beamformer gain drops precipitously is approximately 1300 m^{-3} in a 1 μm bin. The beamformer gain against noise shows a steady decrease with the log of bubble density, but there is no precipitous drop and no critical bubble density. This may indicate that the decrease in mean BG_{noise} is due to increasing bubble attenuation rather than scattering by nearby bubbles.

Figure 9 shows the variance of the phase difference measured between hydrophones 1 and 2 at 30 kHz (i.e., the variance of the histograms in the center column of Fig. 5) plotted against the bubble densities given in Table I for 30 kHz (118 μm bubbles). The theoretical prediction is discussed in the next section. Clearly the variance of the phase difference increases with increasing bubble density. The phase difference variance increases by a modest amount in response to a 500-fold increase in bubble density, but then increases sharply as the density increases by another factor of six. Comparing Figs. 9 and 8 indicates that the reduction in beamformer signal gain is correlated with the increase in phase difference variance. In terms of cause and effect, it makes sense that increased phase variation among the hydrophones is responsible for the reduction in beamformer gain.

V. THEORY AND SIMULATION

A. Description

The measurement results presented in Figs. 8 and 9 indicate that variation in the signal phase among the hydrophones is strongly correlated with the gain achieved by

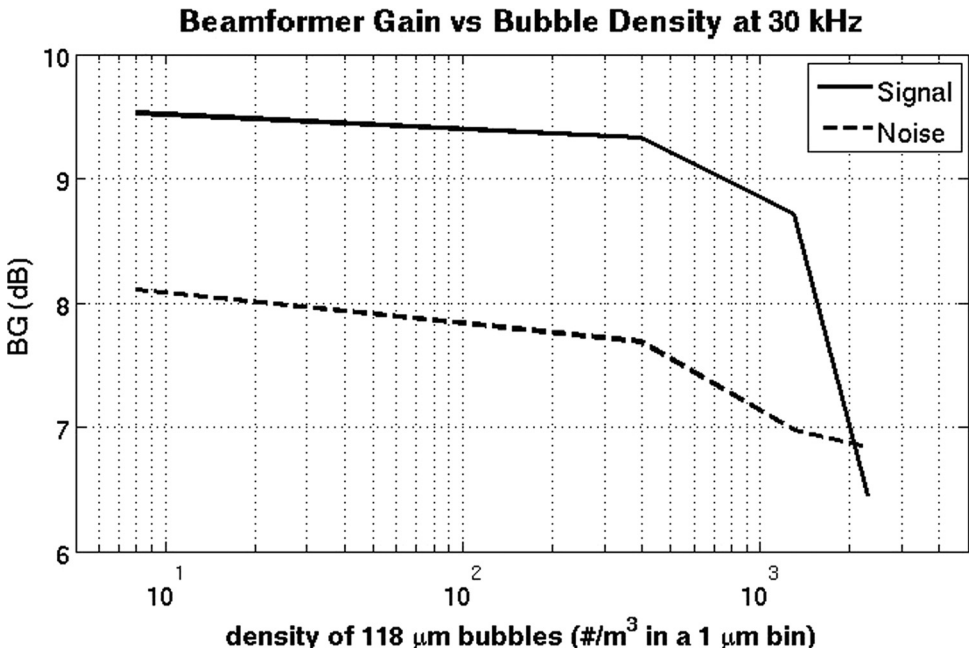

FIG. 8. Mean beamformer gain for the signal and noise at 30 kHz vs bubble densities given in Table I for 30 kHz (118 μm bubbles).

coherent processing (i.e., beamforming) of the hydrophone signals, and that both depend upon the bubble density at the array (the local bubble density). The connection between phase difference and beamformer gain is that phase differences reduce correlation between the signals, and beamformer gain depends upon the signal being correlated and the noise being uncorrelated among the hydrophones. This section presents a theory that quantitatively explains the dependence of phase difference on bubble density and directly links phase difference among the hydrophones to the distance between a bubble and the hydrophones. However, the distances between the bubbles and the hydrophone varies over time because the bubbles are not stationary; they are rising past the hydrophones and the bubble positions change over time and from one transmission to the next. The simulation presented here computes phase and beamformer gain statistics by randomly placing bubbles in the vicinity of the array, taking into account the local bubble density, and computing the effect of the bubbles on signal phase and beamformer gain. The simulation shows that as bubble density at the array increases, the phase variation among the individual hydrophones increases and beamformer gain is degraded at a rate that is consistent with the measurements. Signal attenuation by other bubbles along path from the source to the array is not considered in the simulation because it has an equal effect on all hydrophones for both the direct and bubble scattered signals, and thus does not directly affect array gain.

As discussed previously, an appropriate model for scattering by distributions of bubbles like those considered here is Ishimaru's first order multiple scattering approximation.[5] The simulation geometry is shown in Fig. 10, which is adapted from Ishimaru's Fig. 6-2. The medium is populated with bubbles for $z > 0$. A plane wave is incident from the left at $z < 0$. It propagates to an array of hydrophones located on

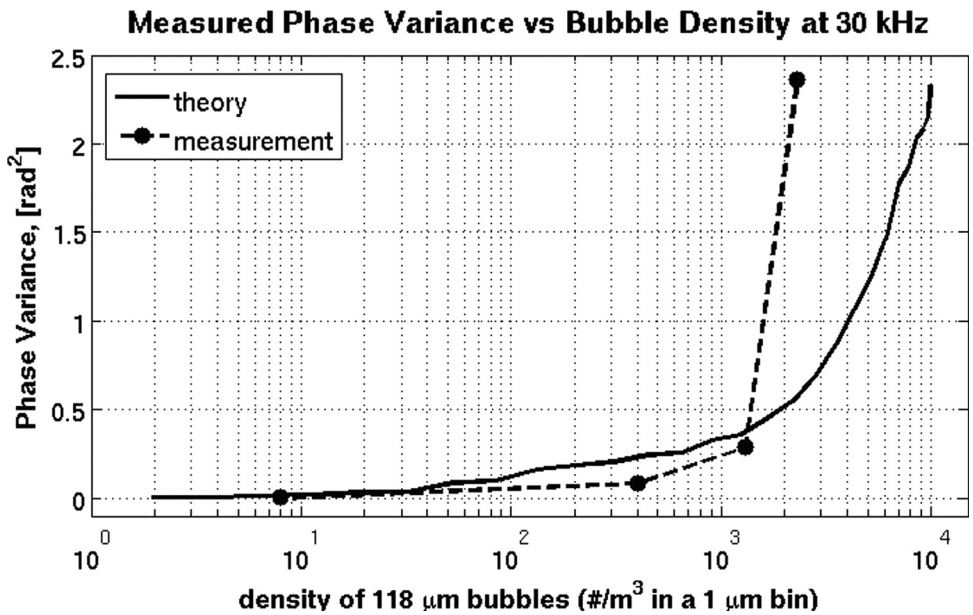

FIG. 9. Variance of the phase difference between two adjacent hydrophones vs measured bubble density. The theoretical prediction is discussed in the next section.

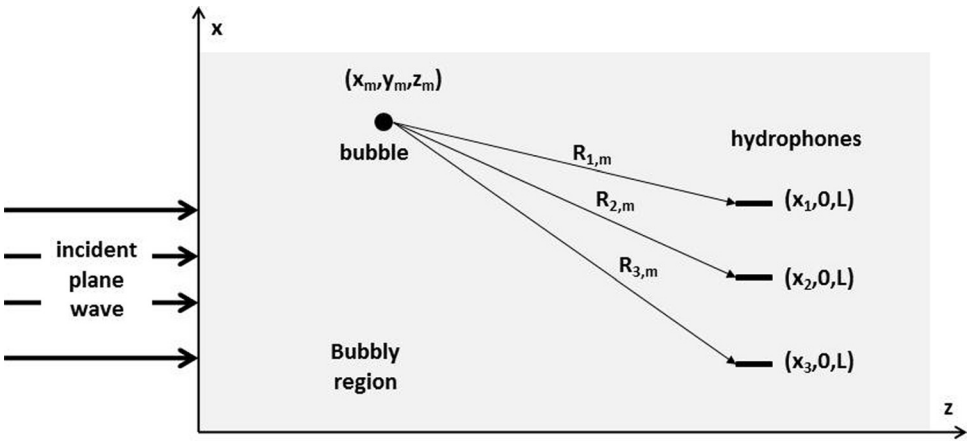

FIG. 10. Plane wave incident on a semi-infinite medium containing bubbles, of which one is shown. The hydrophones are located at $(x_1, 0, L)$, $(x_2, 0, L)$ and $(x_3, 0, L)$.

a vertical line at $z = L$. The plane wave is attenuated by all of the bubbles along the path. The mth resonant bubble located at (x_m, y_m, z_m) is ensonified by the incident field and scatters energy in all directions, including toward the hydrophones. The total signal received by hydrophone j is the sum of the direct path signal and the signals scattered by all bubbles:

$$p_j(t) = \mathrm{Re}\left\{ U_0 \exp(i\omega t) \left[\exp(ikL - \gamma/2) + \sum_{m=1}^{N} \frac{f(\hat{\mathbf{I}}_{j,m}, \hat{\mathbf{O}}_m)}{R_{j,m}} \times \exp\left(ikz_m + ikR_{j,m} - \frac{\gamma_{0,m}}{2} - \frac{\gamma_{j,m}}{2} \right) \right] \right\}. \quad (8)$$

Here, Re indicates the real part of a complex number, U_0 is the plane wave pressure amplitude, ω is radial frequency, k is the acoustic wave number, $R_{j,m}$ is the range from the mth bubble to hydrophone j, and $f(\hat{\mathbf{I}}_{j,m}, \hat{\mathbf{O}}_m)$ is the scattering amplitude of the mth bubble, with $\hat{\mathbf{I}}_{j,m}$ and $\hat{\mathbf{O}}_m$ the incident and scattered directions, respectively. The γ's are the attenuation coefficients (with units of nepers) along the paths from $z = 0$ to $z = L$, from $z = 0$ to $z = z_m$ and from the mth bubble to the jth hydrophone:

$$\gamma = \int_0^L \int_0^\infty \sigma_e(a)\Psi(a)\mathrm{d}a\mathrm{d}z, \quad \gamma_{0,m} = \int_0^{z_m} \int_0^\infty \sigma_e(a)\Psi(a)\mathrm{d}a\mathrm{d}z \quad \text{and} \quad \gamma_{j,m} = \int_0^{R_{j,m}} \int_0^\infty \sigma_e(a)\Psi(a)\mathrm{d}a\mathrm{d}R. \quad (9)$$

$\sigma_e(a)$ is the extinction cross section for the bubble (units are m^2). It is the sum of the absorption cross section $\sigma_a(a)$ and the scattering cross section $\sigma_s(a)$. Also $\Psi(a)$ is the bubble density (with units of m^{-4}). Other variables are defined in Fig. 10. The direct path signal is referred to as the coherent component because it does not change (i.e., remains coherent) between the hydrophones and from one transmission to the next. The sum of the signals scattered by the bubbles is referred to as the incoherent component because it is not coherent among the hydrophones and because small changes in bubble location from one transmission to the next cause the signal at a single hydrophone to change and thus be uncorrelated. Note from Eq. (8) we see that the incoherent component increases in magnitude as the distance from the mth bubble to the jth hydrophone $R_{j,m}$ decreases. The average value of $R_{j,m}$ depends upon bubble density because as density increases, the mean distance between bubbles (and between the bubbles and the hydrophones) decreases. For this reason, increasing bubble density increases the incoherent component in the received signal.

For numerical evaluation, two approximations can be made to Eq. (8). First, γ is approximated as being equal to $\gamma_{0,m}$ for all m. This is a good approximation when the bubble is close to the hydrophone and z_m is approximately equal to L. When the bubble is far from the hydrophone such that L is much different from z_m, the incoherent term is negligible and the approximation has no effect. The second approximation is that $\gamma_{j,m}$ is much less than $\gamma_{0,m}$ and thus can be ignored. This is a good approximation when the bubble is close to the hydrophone and $R_{1,m}$ is small and much less than z_m, and has no effect when $R_{1,m}$ is large and the scattered term is negligible. With these approximations, the total signal received by hydrophone j becomes

$$p_j(t) \approx \mathrm{Re}\left\{ U_0 \exp(i\omega t - \gamma/2) \times \left[\exp(ikL) + \sum_{m=1}^{N} \frac{f(\hat{\mathbf{I}}_{j,m}, \hat{\mathbf{O}}_m)}{R_{j,m}} \exp(ikz_m + ikR_{j,m}) \right] \right\} = \mathrm{Re}\{\tilde{P}_j \exp(i\omega t)\}, \quad (10)$$

where $\tilde{P}_j$ is the complex envelope of the pressure, defined as

$$\tilde{P}_j \equiv U_0 \exp(-\gamma/2) \left[\exp(ikL) + \sum_{m=1}^{N} \frac{f(\hat{\mathbf{I}}_{j,m}, \hat{\mathbf{O}}_j)}{R_{j,m}} \times \exp(ikz_m + ikR_{j,m}) \right]. \quad (11)$$

The summation in Eq. (11) accounts for all the bubbles that scatter sound to the hydrophone. The term in brackets reduces to $\exp(ikL)$ if there are no bubbles, or at least none close to the hydrophone. When bubbles are close to the hydrophone, the incoherent component (second term in brackets) increases. The incoherent component depends upon three quanities: the scattering amplitude $f(\hat{\mathbf{I}}_{1,m}, \hat{\mathbf{O}}_m)$, the distance between the bubble and the hydrophone $R_{j,m}$, and a phase term that depends upon the wave number k and the range $R_{1,m}$. The scattering amplitude is taken to be

independent of incident and scattering angles, a common assumption for bubble scattering. It does have a frequency dependence. From Ref. 13,

$$\left|f(\hat{\mathbf{I}}_{j,m},\hat{\mathbf{O}}_m)\right| = \sqrt{\frac{\sigma_s(f,a)}{4\pi}} \approx \frac{a_{resonant}}{\delta} \tag{12}$$

where $a_{resonant}$ is the radius of the resonant bubble and δ is the bubble damping constant due to reradiation (scattering), thermal and viscous losses. The radius of the resonant bubble was given in Eq. (7). The damping constant is approximately 0.08 for 25 kHz to 35 kHz (see Fig. 6.3.1 in Ref. 1). Using this value and Eq. (7) in Eq. (12) yields scattering amplitudes of approximately 0.002 for 25 kHz to 0.001 for 35 kHz. For the incoherent component to become important, $R_{1,m}$ must be less than or equal to this value. In other words, when the bubble-to-hydrophone distance is much larger than 0.002 m, the coherent component will be dominant and the incoherent component will be insignificant. However, as the distance approaches 0.002 m, the incoherent component will become more important.

The simulation utilizes the expression in Eq. (11) to compute the complex amplitude and phase of the signal produced at each hydrophone in a three-element vertical line array with 0.025 m spacing. The voltage corresponding to pressure $\tilde{P}_j$ is denoted $\tilde{V}_j$. A Monte Carlo simulation is carried out in which the positions of a large number of bubbles are randomly selected using a spatially uniform distribution that is consistent with a given density. The number of bubbles simulated increases with density. Each hydrophone receives an identical direct path signal. The bubbles also receive the same incident signal, which is then propagated to the hydrophones using the second term in brackets in Eq. (11). The bubble scattered signals received by each hydrophone are summed coherently with the direct path signal. The total power of the signal received by the jth hydrophone is $\left|\tilde{V}_j\right|^2$, and the power at the beamformer output is $\left|\tilde{V}_1+\tilde{V}_2+\tilde{V}_3\right|^2$.

B. Results

Figure 11 shows histograms of the simulation results. The left column shows distributions of the difference in signal phase at adjacent hydrophones. Bubble density is increasing from bottom to top. Similar to the measurement results shown previously, phase difference in the simulation

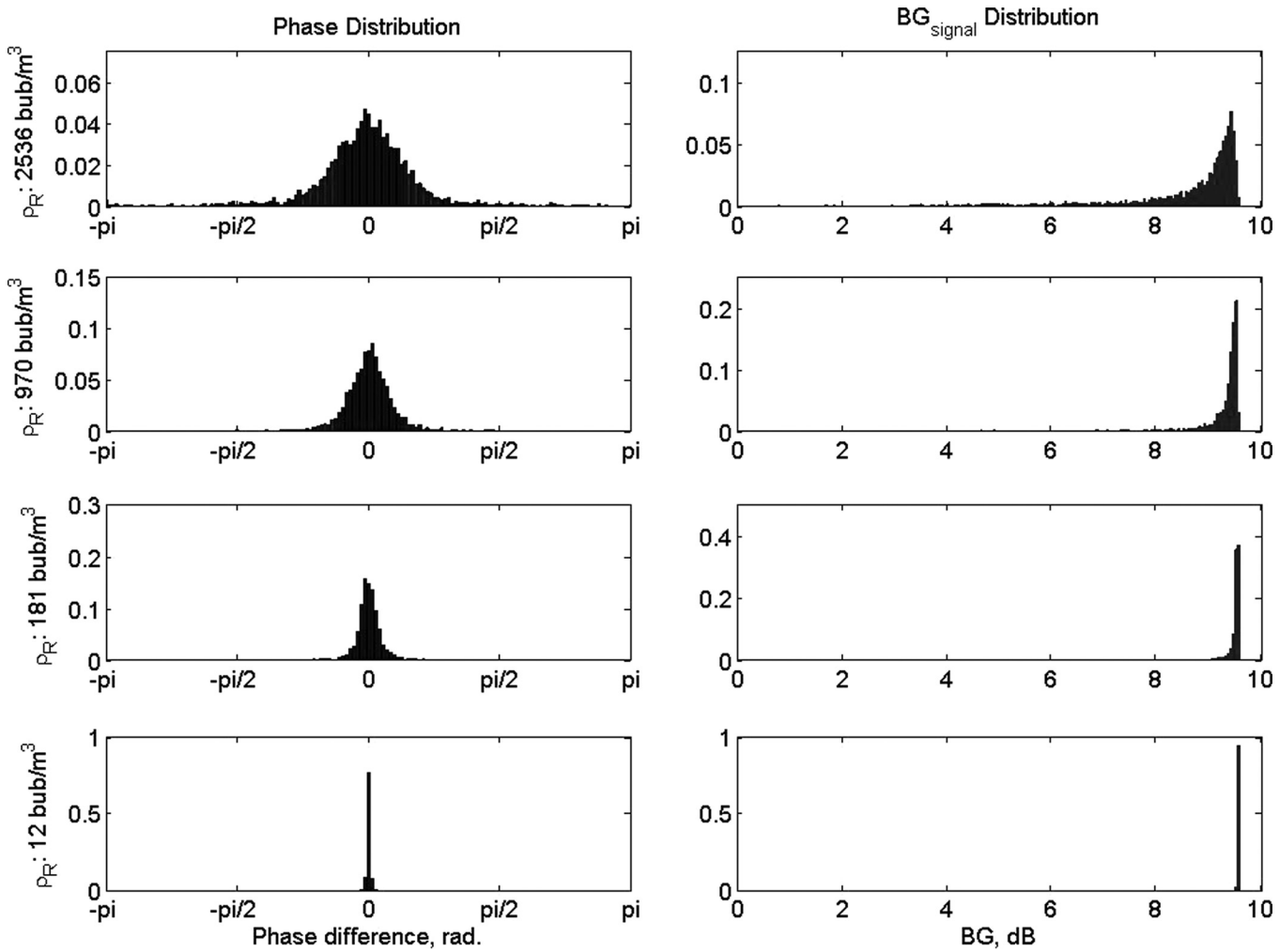

FIG. 11. Results of simulation. Panels in the left column show histograms of the difference in signal phase at adjacent hydrophones. The right column shows histograms of beamformer gain BG_{signal}, in dB. In both columns, bubble density is increasing from bottom to top. Note that the vertical scales are different among the panels.

result becomes more variable with increasing bubble density. Starting from essentially a delta function, the distribution evolves into a flatter von Mises form, and for higher bubble densities the distribution approaches a uniform distribution. The right column shows distributions of BG_{signal} for the same bubble densities. Here again the simulation results display the same trends seen in the measurements. Starting from essentially a delta function, the distribution flattens out as bubble density increases.

The upper panel of Fig. 12 compares measurements and simulation results for the AG that would be achieved by a three hydrophone array operating in bubbly water in the presence of uncorrelated noise. The measurement results are computed using Eq. (3) with the values for BG_{signal} taken from Fig. 8 and BG noise = 4.75 dB, the theoretical prediction for beamformer gain against uncorrelated noise. The theory/simulation curve is $10 * \log_{10}(|\tilde{V}_1 + \tilde{V}_2 + \tilde{V}_3|^2)$ minus 4.75 dB. The theory compares favorably with the first three measured values up to a density of about 1100 bubbles/(m^3 · μm). For higher bubble densities, the theory predicts that the decrease in AG with increasing density is not as rapid as that reflected by the measurements. Further discussion of these results, as well as the bottom panel in Fig. 12 are discussed in the next section.

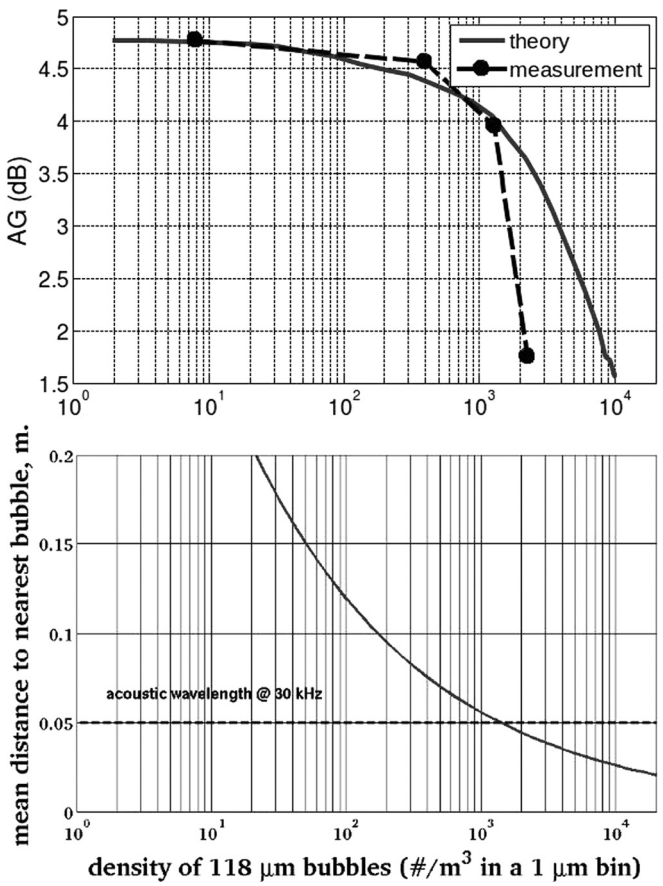

FIG. 12. (Upper) Mean AG at 30 kHz from measurements and simulation. The measurement result utilizes Eq. (3) with the BG_{signal} taken from Fig. 8 and $BG_{\text{noise}} = 4.75$ dB, the theoretical prediction for uncorrelated noise. The theory/simulation prediction is $10 * \log_{10}(|\tilde{V}_1 + \tilde{V}_2 + \tilde{V}_3|^2)$ minus 4.75 dB. (Lower) Mean distance between resonant bubbles calculated using an expression derived in the Appendix. The acoustic wavelength at 30 kHz is also shown for comparison.

VI. DISCUSSION

The upper panel of Fig. 12 shows that the theory is consistent with the 30 kHz measurements in predicting that AG falls off rapidly with increasing bubble density beginning around 1000 – 2000 bubbles/(m^3 · μm). The theory and numerical simulation calculates phase variation among the hydrophones due to scattering from nearby bubbles and predicts an increase with increasing bubble density. Array gain computed from the numerical simulation output is shown to be degraded when phase variation increases and signal correlation among the hydrophones drops. That the theory predicts the same trend seen in the measurements lends some credence to this mechanism.

However, the theoretical prediction and the measurements are inconsistent for the highest density in the upper panel of Fig. 12. Our suspicion is that the theory is correct, but that the largest bubble density measurement, against which the lowest measured values of BG and AG are plotted, is in error. As discussed previously, the resonant bubble densities at the locations of the AG measurements were estimated from an entirely separate set of acoustic attenuation measurements. If the highest bubble density measurements are erroneously low, then the values of AG corresponding to the highest density would be plotted vs an erroneously low density value. For the 4th data point, the estimated density appear to be a factor of 5 low.

An indication of why bubble density might be under estimated can be found in Clay and Medwin,[1] who cite Ref. 14 and state that "When scatterers are packed together closely enough for their scattered fields to interact, … the result of the interaction is that the resonance curve of a single bubble is broadened and the scattering cross section of a group of bubbles is less than the sum of the individual cross sections." Interaction begins to occur at separations equal to a wavelength.

It is shown in the Appendix that the expected distance between the hydrophone and the nearest bubble is approximately $0.554 * (\Psi(a)\Delta a)^{-1/3}$, where Δa is the bubble resonance width. The mean hydrophone-bubble minimum distance is plotted in the lower panel of Fig. 12 as a function of bubble density. Note that the mean distance is 0.05, which is the acoustic wavelength at 30 kHz, when the bubble density is about 1400 m^{-3} in a 1 μm bin. This is consistent with the point at which the simulation and measurements begin to diverge in the upper panel of Fig. 12.

As discussed by Clay and Medwin, the effect of interaction between the bubble is to broaden the resonance peak. The width of the resonant peak is inversely proportional to the quality factor Q and proportional to the damping constant δ. Since the extinction cross section at resonance is proportional to δ^{-2}, interaction will cause this quantity to decrease. A two-fold increase in δ will produce a four-fold decrease in extinction cross section. If the extinction cross section used to estimate bubble density from measured attenuation is a factor of four higher than the true value, then the bubble density estimate will be low by a factor of four. To summarize, the idea is that the lowest measured value of AG shown in Fig. 12, about 1.75 dB, has been plotted vs an erroneously low bubble density. Moving this point to the right by a factor

of five would bring the measurement curve into much better agreement with the theory.

Another other possible explanation for the model-measurement divergence is that the "first-order multiple scattering" model used in the simulation breaks down at higher bubble density and fails to predict the amount of phase variability corresponding to a particular bubble density. In fact, the simulation does predict less phase variability between the hydrophones than that observed in the AG measurements, as can be seen in Fig. 9. However, the bubble density estimation error discussed above would also cause the measured phase variance to be plotted vs an erroneously low density value in Fig. 9. Correcting this error would bring the phase variation measurement into agreement with the simulation. Also, as discussed earlier, two of the possible three conditions for validity of the "first-order multiple scattering" approximation are satisfied by the experimental conditions. Thus, it seems likely that the model remains a valid approximation for the present measurement results.

One aspect of the theory/simulation which may contribute to errors is that the receive hydrophone is taken to consist of a single point. The finite size of the hydrophone active element, if properly accounted for, would in many cases reduce the distance between a bubble and hydrophone. From Eq. (11), reducing R would increase the contribution of scattering by the bubbles, increasing the phase variation and lowering the AG, potentially improving the agreement between theory and measurement.

VII. SUMMARY AND CONCLUSIONS

The effects of the nearby air bubbles on the gain achieved by beamforming with an array of underwater hydrophones has been measured and investigated theoretically. Measurements using a three hydrophone line array show that received signal phase variance and array gain (AG) are dependent on the bubble density near the array. Histograms of measured phase differences between the receive signals indicate that phase variability increases with increasing bubble density at the array, reducing correlation among the received signals and causing AG to be reduced. A theory and simulation have been developed that directly connect the AG provided by a hydrophone array to the density of nearby resonant bubbles. The numerical simulation calculates the effect of scattering by nearby bubbles on phase variation and signal correlation, and the results compare favorably with measured phase variation. The simulation predicts AG degradation with increasing bubble density that is quantitatively the same as the measured AG for all but the highest density measured.

There appears to be some difference between the bubble density estimate at the location where AG was most degraded and the density at which degradation is predicted to occur. Bubble density was measured separately from the AG measurements, and there is some evidence that the highest bubble density may have been under estimated. This kind of error reportedly occurs at densities for which the average distance between bubbles is roughly equal to the acoustic wavelength, as was the case here. At higher bubble densities, when interaction occurs between the bubbles, the resonance peak flattens out and the extinction cross section is reduced. Since bubble density estimates are obtained by dividing the measured attenuation by the extinction cross section, using an erroneously high cross section will result in an erroneously low bubble density estimate.

The most important result of this paper is as follows. Except at the highest bubble density, the simulation results quantitatively agree with the phenomena observed in the measurement. The simulation is therefore capable of predicting the effect of specific bubble densities on the gain that that an array can produce. In answer to the question that motivated this study, the measurement and simulation results indicate that the effects of the bubbly wake on the AG provided by a line array of hydrophones towed at shallow depth behind a surface ship go beyond attenuation. Scattering by bubbles close to the array has been shown to reduce signal correlation across the array and in turn reduce the AG. Specifically, the theory and simulation provide a means of predicting how shallow an array can be towed behind a surface ship with known wake acoustic characteristics without compromising the gain available from the array. It would be interesting to validate these predictions with full-scale data. It would also be interesting to further investigate how higher bubble density and multiple scattering affect the extinction cross section of resonant bubbles.

ACKNOWLEDGMENTS

Two of the authors (R.L.C. and J.D.P.) gratefully acknowledge the support of Mike Vaccaro at the Office of Naval Research. The work of Paul Doust, D.N.V., UK to match the transducer and amplifier over a broad frequency range is appreciated. Fred Holt calculated bubble densities from the attenuation measurements.

APPENDIX: MEAN DISTANCE BETWEEN BUBBLES

Consider a three-dimensional space in which resonant bubbles are randomly distributed with known bubble density $\rho = \Psi(a)\Delta a$, where Δa is the bubble resonance width. The units of ρ are m^{-3}. We want to calculate the mean value of R, the distance from an arbitrary point (e.g., the origin) to the nearest bubble. This calculation requires knowledge of the probability distribution function of R.

Begin by writing the cumulative distribution function of R:

$$F_R(r) = \mathrm{Prob}(R \leq r) = 1 - \mathrm{Prob}(R > r). \tag{A1}$$

$\mathrm{Prob}(R > r)$ is the probability that there are no bubbles within a distance r from the origin. In general, the probability that there are k bubbles in volume V (no relation to the wavenumber k used previously) follows a spatial Poisson process described by Ref. 15:

$$\mathrm{Prob}(k \text{ bubbles in volume } V) = \frac{(\rho V)^k e^{-\rho V}}{k!}. \tag{A2}$$

Note that the average number of bubbles in volume V is ρV. Setting $k = 0$ in Eq. (A2) and setting $V = (4/3)\pi r^3$ gives

$$\text{Prob}(R > r) = \text{Prob}\left(\text{no bubbles in volume } V = \frac{4}{3}\pi r^3\right) = \exp\left(-\frac{4}{3}\pi r^3 \rho\right). \quad \text{(A3)}$$

The probability density function of R is

$$f_R(r) = \frac{\mathrm{d}F_R(r)}{\mathrm{d}r} = 4\pi r^2 \rho \exp\left(-\frac{4}{3}\pi r^3 \rho\right). \quad \text{(A4)}$$

The distance from the origin to the nearest bubble is distributed according to Eq. (A4). The expected value of this distance is

$$E[R] = \int_0^\infty r f_R(r)\mathrm{d}r = \frac{\Gamma\left(\frac{4}{3}\right)}{\left(\frac{4}{3}\pi\rho\right)^{1/3}} \approx 0.554^* \rho^{-1/3}. \quad \text{(A5)}$$

Similar analyses can be performed for the 1-D and 2-D cases. The result for 2-D is

$$E[R] = \int_0^\infty r\rho\pi r \exp(-\rho\pi r^2)\mathrm{d}r = \frac{\Gamma\left(\frac{3}{2}\right)}{(\pi\rho)^{1/2}} \approx 0.5^* \rho^{-1/2} \quad \text{(A6)}$$

and for 1-D

$$E[R] = \int_0^\infty r\rho \exp(-\rho r)\mathrm{d}r = \frac{\Gamma\left(\frac{2}{1}\right)}{(\rho)} = \frac{1}{\rho}. \quad \text{(A7)}$$

1. Distribution of *r* using order statistics

Another approach involves the use of order statistics. Consider a geometry in which N points are randomly distributed within a sphere with radius R. Each of the points is independent and identically distributed with a known density. We are interested in the distribution function in the radial direction, $f_R(r)$. Since global density is assumed to be constant, the enclosed number of bubbles is proportional to the volume. Therefore, the distributions in the radial direction are

$$F_R(r) = \frac{r^3}{R^3}, \quad \text{(A8)}$$

$$f_R(r) = \frac{\mathrm{d}F_R(r)}{\mathrm{d}r} = \frac{3r^2}{R^3}. \quad \text{(A9)}$$

Using order statistics,[16] the distributions of the minimum distance is expressed as

$$f_{R_{min}}(r) = N[1 - F_R(r)]^{N-1} f_R(r) \quad \text{(A10)}$$

Using Eqs. (A9), (A8) and substituting $N = \rho\left(\frac{4\pi R^3}{3}\right)$, and Eq. (A10) can be written as

$$f_{R_{min}}(r) = \rho\frac{4\pi R^3}{3}\left(1 - \frac{r^3}{R^3}\right)^{(\rho 4\pi R^3/3)-1}\frac{3r^2}{R^3}. \quad \text{(A11)}$$

For an infinite space with density ρ we take the limit of Eq. (A11)

$$\lim_{R\to\infty} \rho\frac{4\pi R^3}{3}\left(1-\frac{r^3}{R^3}\right)^{(\rho 4\pi R^3/3)-1}\frac{3r^2}{R^3} = \rho 4\pi r^2 \exp\left(-\rho\frac{4\pi r^3}{3}\right). \quad \text{(A12)}$$

This is identical to Eqs. (A4) and (A5) follows directly.

[1] C. S. Clay and H. Medwin, *Acoustical Oceanography: Principles and Applications* (Wiley, New York, 1977), Chap. 6.
[2] A. Ishimaru, *Wave Propagation and Scattering in Random Media* (IEEE, New York, 1997), Chap. 3.
[3] W. S. Burdick, *Underwater Acoustic System Analysis* (Peninsula Publishing, Los Altos, CA, 2002), Chap. 11.
[4] R. J. Urick, *Principles of Underwater Sound*, 3rd ed. (Peninsula Publishing, Los Altos, CA, 1983), Chap. 3.
[5] A. Ishimaru, *Wave Propagation and Scattering in Random Media* (IEEE, New York, 1997), Chaps. 4 and 6.
[6] M. A. Ainslie and T. G. Leighton, "Near resonant bubble acoustic cross-section corrections, including examples from oceanography, vocanology, and bimedical ultrasound," J. Acoust. Soc. Am. **126**, 2163–2175 (2009).
[7] R. L. Culver and M. F. Trujillo, "Effects of scattering by air bubbles on performance of an underwater array," J. Acoust. Soc. Am. **121**, 3033 (2007).
[8] T. G. Leighton, D. C. Finfer, P. R. White, G. H. Chua, and J. K. Dix, "Clutter suppression and classification using twin inverted pulse sonar (TWIPS)," Proc. R. Soc. London **466**, 3453–3478 (2010).
[9] A. P. Martins, "A DFT-based phasor estimation method for power electronics converter control and protection under strong grid voltage perturbations," Eur. Trans. Electr. Power **19**(8), 1082–1097 (2009).
[10] R. Barakat, "Direct derivation of intensity and phase statistics of speckle produced by a weak scatterer from the random sinusoid model," J. Opt. Soc. Am. **71**(1), 86–90 (1981).
[11] R. Barakat, "Weak-scatterer generalization of the K-density function. II. Probability density of total phase," J. Opt. Soc. Am. A **4**(7), 1213–1219 (1987).
[12] J. W. Caruthers, P. A. Elmore, J. C. Novarini, and R. R. Goodman, "An iterative approach for approximating bubble distributions from attenuation measurements," J. Acoust. Soc. Am., **106**, 185–189 (1999).
[13] A. Ishimaru, *Wave Propagation and Scattering in Random Media* (IEEE, New York, 1997), Eqs. (2-4) and (3-19).
[14] D. Weston, "Acoustic interaction effects in arrays of small spheres," J. Acoust. Soc. Am. **39**, 316–312 (1966).
[15] A. Baddeley, *Case Studies in Spatial Point Process Modeling* (Springer-Verlag, New York, 2006).
[16] A. Papoulis, and S. U. Pillai, *Probability, Random Variables and Stochastic Processes* (McGraw-Hill, New York, 2002), Chap. 7.